BBA - Molecular Basis of Disease 1865 (2019) 126–135

Contents lists available at ScienceDirect

BBA - Molecular Basis of Disease

journal homepage: www.elsevier.com/locate/bbadis

Deficiency of the mitochondrial sulfide regulator ETHE1 disturbs cell growth, glutathione level and causes proteome alterations outside mitochondria

Navid Sahebekhtiari, Paula Fernandez-Guerra, Zahra Nochi, Jasper Carlsen, Peter Bross, Johan Palmfeldt*

Research Unit for Molecular Medicine, Department of Clinical Medicine, Aarhus University and Aarhus University Hospital, Palle Juul-Jensens Boulevard 99, DK-8200 Aarhus N, Denmark

ARTICLE INFO

Keywords:
Ethylmalonic encephalopathy
Sulfide
Glutathione
Glycosylation
Redox regulation
Mitochondrion

ABSTRACT

The mitochondrial enzyme ETHE1 is a persulfide dioxygenase essential for cellular sulfide detoxification, and its deficiency causes the severe and complex inherited metabolic disorder ethylmalonic encephalopathy (EE). In spite of well-described clinical symptoms of the disease, detailed cellular and molecular characterization is still ambiguous. Cellular redox regulation has been described to be influenced in ETHE1 deficient cells, and to clarify this further we applied image cytometry and detected decreased levels of reduced glutathione (GSH) in cultivated EE patient fibroblast cells. Cell growth initiation of the EE patient cells was impaired, whereas cell cycle regulation was not. Furthermore, Seahorse metabolic analyzes revealed decreased extracellular acidification, i.e. decreased lactate formation from glycolysis, in the EE patient cells. TMT-based large-scale proteomics was subsequently performed to broadly elucidate cellular consequences of the ETHE1 deficiency. More than 130 proteins were differentially regulated, of which the majority were non-mitochondrial. The proteomics data revealed a link between ETHE1-deficiency and down-regulation of several ribosomal proteins and LIM domain proteins important for cellular maintenance, and up-regulation of cell surface glycoproteins. Furthermore, several proteins of endoplasmic reticulum (ER) were perturbed including proteins influencing disulfide bond formation (e.g. protein disulfide isomerases and peroxiredoxin 4) and calcium-regulated proteins. The results indicate that decreased level of reduced GSH and alterations in proteins of ribosomes, ER and of cell adhesion lie behind the disrupted cell growth of the EE patient cells.

1. Introduction

Determining the dynamic links between genotype and phenotype of inherited metabolic disorders is challenging, meanwhile indispensable for understanding disease mechanisms. Since many of these disorders have serious clinical symptoms and multiple biochemical traits, detailed molecular characterization is necessary for elucidating disease mechanism and for finding new putative treatment approaches. Large-scale proteomics—analyzing hundreds or even thousands of proteins—is a strong tool for such molecular characterization [1,2]. Ethylmalonic encephalopathy, EE (OMIM No. 602473) is a fatal, rare autosomal recessively inherited metabolic disorder caused by genetic variation in the gene *ETHE1*. The *ETHE1* gene encodes a mitochondrial persulfide dioxygenase, which is involved in sulfide detoxification [3]. Loss of function mutations in the *ETHE1* gene lead to sulfide accumulation and causes a combination of biochemical and clinical symptoms, such as severe deficiency of cytochrome *c* oxidase (COX) in brain and muscle, high levels of C4 and C5 acylglycines, high excretion of ethylmalonic acid (EMA), petechiae, acrocyanosis, and neurodevelopmental delay [3–6]. The high level of excreted EMA has been ascribed to originate from inhibition of short-chain acyl-CoA dehydrogenase (SCAD) by high sulfide levels [3]. This explains the partial overlap in protein alteration in ETHE1-deficient and SCAD deficient patients [7]. A mouse proteomics study described the impact of ETHE1 deficiency on several different pathways within the cell, such as fatty acid β-oxidation, cytoskeleton and branched chain amino acid catabolism [8]. Another proteomics study, on livers from ETHE1 deficient mice described alterations in several redox-related proteins, including liver specific cytochrome P450 proteins and glutathione S-transferases, in addition to increased amounts of metabolic enzymes, both from β-

* Corresponding author.
E-mail address: johan.palmfeldt@clin.au.dk (J. Palmfeldt).

https://doi.org/10.1016/j.bbadis.2018.10.035
Received 24 May 2018; Received in revised form 14 October 2018; Accepted 30 October 2018
Available online 02 November 2018

oxidation and pyruvate metabolism [9]. In mitochondria from human ETHE1 deficient fibroblast cells only few proteins were found to be regulated, although changes in oxidoreductases indicate redox perturbation [6]. These findings call for further elucidation, since ETHE1 apparently has effects on cellular biochemistry and cellular proteome that goes beyond inhibition of COX and SCAD.

We therefore set out to study the changes in physiology and proteome of cultured human dermal fibroblasts derived from skin biopsies of ETHE1-deficient patients with ethylmalonic acid encephalopathy (hereafter referred to as "EE cells"). These cultured EE cells have less pronounced biochemical phenotype, i.e. less degree of COX and SCAD inhibition, than observed in tissue samples, which likely is explained by the oxygen rich environment favoring sulfide detoxification by oxidation [3]. The EE cells can thus serve as a good model to study milder effects of ETHE1 deficiency, and cultivated fibroblasts are suitable for both functional studies and for proteomics. Furthermore, the link between ETHE1 and sulfide, and the functional role of sulfide in redox regulation [10] encouraged us to investigate the redox state in living EE cells, by measuring reduced glutathione (GSH) with image cytometry [11] as well as metabolic activities of the cells. Our comprehensive quantitative proteomics data highlight alterations in pathways previously not described in the context of ETHE1 deficiency, and shows that ETHE1 deficiency has pervasive physiological effects.

2. Materials and methods

2.1. Patient and control samples

Primary human dermal fibroblasts from three ethylmalonic encephalopathy (EE) patients ("EE cells") and three healthy controls ("control cells") were included in this study, and all of them were included in the measurements of the various analytical parameters. EE cells were from three patients diagnosed with EE, caused by exon 4 deletion in ETHE1. The mutation causes lack of ETHE1 protein as previously described together with patient symptoms [6]. The three healthy individuals were from newborn males (Cambrex #CC-2509, ATCC #CRL-2429, and ATCC #CRL-2450). The samples were de-identified according to regulations of The Danish Ethical Committee.

2.2. Cell culturing

The fibroblasts were cultured in Dulbecco's Modified Eagle Media (DMEM) (Lonza, Denmark) supplemented with 2 mmol/L of L-glutamine (Leo Pharmaceutical, Denmark), 10% fetal bovine serum (Invitrogen, USA), and 0.1% penicillin/streptomycin (Leo Pharmaceutical, Denmark). Fibroblasts derived from patients and healthy individuals were cultured under mycoplasma-free conditions. Cells were harvested by trypsinization at 75–85% confluence. The proteomics experiments were entirely replicated two times, at different time points, whereas image cytometry and Seahorse based assays were entirely replicated three times. The number of cell passages was between eight and thirteen for all experiments except for one of the cell count experiments in Fig. 2, which had sixteen passages.

2.3. Sample preparation

Approximately 2.0×10^7 cells were harvested and resuspended in five cell-pellet volumes of Lysis Buffer from TMT Mass Tagging Kits and Reagents (Thermo Fisher Scientific, USA) with Complete protease inhibitor cocktail tablets (Roche Diagnostic Gmbh, Germany). The cell suspension was ultrasonicated (Branson Sonifier 250, Branson Ultrasonics Corp, USA) on ice, at output 3 and 30% duty cycle for four rounds of 10 pulses with 1 min on ice between each round. Protein concentration was measured by the Bradford assay (Bio-Rad, USA).

2.4. Preparing and labeling peptides with the TMT Isobaric Mass Tags

In each of the two independent TMT studies, equal amounts of proteins (100 μg) from the six different fibroblast samples were processed according to TMT 6-plex manufacturer's instructions. Briefly, each sample was reduced and alkylated with 200 mmol/L tris (2-carboxyethyl) phosphine (TCEP) and 375 mmol/L iodoacetamide, respectively. Subsequently were the protein samples precipitated with acetone (−20 °C, overnight), followed by protein digestion with 2.5 μg Trypsin supplied by the kit. After peptide labeling, with TMT label reagents, the peptide samples of the three patients and the three healthy individuals were pooled. Pooled peptides were purified on PepClean C-18 Spin Columns (Pierce, Thermo Fisher Scientific, USA) prior to peptide separation by isoelectric focusing (IEF) on Multiphor II unit (Pharmacia Biotech AB, Sweden) using 18 cm Immobiline Drystrip Gradient (IPG) pH 3–10 gel (GE Healthcare, Sweden). Samples were rehydrated for 16 h in rehydration buffer containing 8 mol/L Urea, 0.5% IPG buffer (GE Healthcare) and 0.002% bromophenol blue. IEF was run with the following gradient program: 1 min gradient from 0 to 500 V, 1.5 h gradient from 500 to 3500 V, followed by 3500 V for 16 h. The IPG strip was cut into 8 pieces of equal size and then peptides were extracted from the IPG strip with 5% acetonitrile (AcN) and 0.5% trifluoro acetic acid (TFA). Extracted peptides were purified by PepClean C-18 spin columns according to manufacturer's instruction prior to nLC mass spectrometry.

2.5. Nano- liquid chromatography tandem mass spectrometry (nLC-MS/MS) analysis

The peptide mixtures were analyzed by nano-liquid chromatography tandem mass spectrometry (nanoLC-MS/MS) (EASY nanoLC-1000, Thermo Scientific) coupled to Q Exactive™ Plus Hybrid Quadrupole-Orbitrap™ Mass Spectrometer (Thermo Fisher Scientific). TMT labelled peptide samples were trapped on a pre-column (PepMap 100, 2 cm, 75 μm i.d., 3 μm C18 particles, 100 Å, Thermo Scientific) followed by reverse phase separation on a C18 column with integrated emitter (EASY-Spray column, PepMap 25 cm, 75 μm i.d., 2 μm, 100 Å, Thermo Scientific). Peptides were separated in a 90 min linear gradient, from 4 to 40% acetonitrile in 0.1% formic acid at a flowrate of 300 nL/min. The MS was operated in a positive, data dependent mode, automatically switching between precursor scanning (MS1) and fragmentation (MS2) acquisition. Resolution of MS1 was set to 70,000 and MS2 to 35,000. In MS1, automatic gain control (AGC) target was set to 1×10^6 ions and scan range between 380 and 1800 m/z. In MS2, AGC target was set at 2×10^5 ions, with fixed first mass set to 120 m/z. Dynamic exclusion was set to 20 s for all analyses. Up to ten of the most intense ions were fragmented per every full MS scan, by higher-energy C-trap dissociation (HCD). Ions with single charge or unassigned charge states were excluded from fragmentation.

2.6. Database searches and statistics

The raw data files from two separate TMT studies were processed. In each TMT study all 8 peptide fractions were analyzed twice, first by standard analysis and then in an extra MS run applying exclusion lists of the abundant peptides (> 10 fragment scans). Later all of the generated peak lists from the same study were merged and analyzed by Mascot version (2.5.1) (Matrix Science, UK) in Proteome Discoverer 1.4 (Thermo Fisher Scientific). SwissProt database released 2014_10 containing 20,194 review protein sequences and Mascot was used for protein identification as well as TMT reporter quantification. Full scan tolerance was 8 ppm, MS/MS tolerance was 30 mmu, minimum peak count was 20, maximum precursor co-isolation was 40%, and maximum of missed trypsin cleavages was 2. Oxidation on methionine was set as dynamic modification while TMT 6-plex on lysine and N-terminal, and carbamidomethyl on cysteine were chosen as static modifications.

Normalization to summed intensities of TMT signal was applied to compensate for possible variation in starting material. We only considered proteins with identification score ≥ 30 (corresponding to protein identification significance of 0.001) and with at least three peptides scans for each protein.

2.7. Bioinformatic and data analysis

Two separate TMT studies were performed for each cell line, and the proteins common for both studies were selected for further bioinformatics analyses. The final list of significantly regulated proteins was based on two criteria. First, the *t*-test statistics should have a probability value below 0.05 in at least one study, and not higher than 0.1 in the second one. Second, the ratio of the average of TMT values from ETHE1-deficient cells to the average from healthy controls, for each protein which passed the first criteria, should have a value higher than 1.3 or below 0.76 (i.e. fold change > 1.3). Hierarchical clustering based on the correlations of expression profiles of all cell lines was performed on quantified proteins using software Cluster 3.0 (http://bonsai.hgc.jp/~mdehoon/software/cluster/) and Java TreeView (http://jtreevie.sourceforge.net/) [12,13]. To obtain functional annotation of the significant proteins we used the online bioinformatic tool DAVID (Database for Annotation, Visualization and Integrated Discovery) version 6.8 [14]. The total list of common proteins identified in both studies was used as background list (n = 3562) (Supplementary Table S1). We include clusters with an enrichment score above 1.12 corresponding to $p < 0.075$ for cluster probability, see Table 1 and Supplementary Tables S3 and S4.

The mass spectrometry proteomics data have been deposited to the ProteomeXchange Consortium via the PRIDE [15] partner repository with the dataset identifier PXD009880.

2.8. Western blotting

Protein expression levels of four proteins; adenylate Kinase 4 (AK4), endoplasmic reticulum chaperone BiP (HSPA5, or GRP78), protein disulfide-isomerase (PDIA1, or P4HB) and peroxiredoxin 4 (PRDX4), were evaluated by western blotting. Protein extracts were prepared from a new set of cultivations (passage numbers < 13), compared to the ones studied by TMT-based proteomics, and protein concentrations were determined using a Pierce™ BCA Protein Assay Kit (Thermo Fisher Scientific). Approximately 20 μg (PDIA1 and PRDX4) or 40 μg (AK4 and BiP) protein from each sample was separated by SDS-PAGE on an Any kD™ Criterion™ TGX Stain-Free™ Protein Gel (Biorad). The protein was transferred from the gel by semi-dry blotting to a polyvinylidene difluoride (PVDF) membrane by application of the Trans-Blot® Turbo™ RTA Midi LF PVDF Transfer Kit using Trans-Blot® Turbo™ Transfer Apparatus (both from Biorad). Next, the membrane was UV-activated for 4 min and imaged for evaluation of total protein with a LAS4010 Imaging system (GE Healthcare). Subsequently the membranes were incubated over night with one of the following primary antibodies: polyclonal rabbit anti-human Adenylate kinase 4 (LSBio #LS-C31854, 1:1000 dilution), polyclonal rabbit Anti-GRP78 BiP antibody (Abcam #ab191023, 1:2500 dilution), monoclonal rabbit Anti-P4HB antibody (Abcam #ab137119, 1:4000 dilution), polyclonal rabbit PRDX4 antibody (Thermo Fisher Scientific #PA3-753, 1:4000 dilution). The membrane was washed in PBS and incubated for 1 h with a secondary goat anti-rabbit antibody (Dako #P0448, 1:20,000 dilution). Finally, they were developed using the Pierce™ ECL Plus Western Blotting Substrate (Thermo Fisher Scientific #32132) and the LAS4010 Imaging system was applied to record the chemifluorescence signal from the membranes corresponding to the levels of the specific proteins. Total and specific protein signals were obtained using ImageQuant TL 7.0 software (GE Healthcare).

2.9. Phenotypic characterization by image cytometry

Measurements of cellular fluorescence were performed with NC-3000 image cytometer (Chemometec, Denmark) on fibroblasts from patients and healthy controls at 70–80% confluence. Thiol Redox Status (TRS), mitochondrial membrane potential (MMP), and viability assays were performed and analyzed as previously described [16]. Briefly, for TRS, VitaBright-48 (VB-48) was used to measure the level of reduced thiol groups [17]. VB-48, propidium iodide (PI) and acridine orange (AO) were added to cells. The analysis was performed according to the "Vitality protocol" from NC-3000. For MMP assay, cells were incubated with 5,5′,6,6′-tetrachloro-1,1′,3,3′-tetraethylbenzimidazolylcarbocyanine iodide (JC-1) for 10 min. Carbonyl cyanide 3-chlorophenylhydrazone (CCCP) was used to determine the mitochondrial membrane potential depolarization. For viability assay, cells were mixed with lysis buffer (1:1) and DAPI (25 μg/mL) to count the total cell amount (Ct). To count the non-viable cells (Cnv), DAPI (25 μg/ml) was added followed by

Table 1
Clusters of differentially regulated proteins with functional overrepresentation. DAVID functional annotation tool was applied on the 88 up-regulated proteins (A) and 44 down-regulated (B). Count denotes the number of proteins (HGNC gene names to the right) in the respective cluster. See Supplementary Tables S3 and S4 for complete cluster data output of up- and down-regulated, respectively.

Cluster	Description of term	Count	p-Value	Proteins in the cluster
A. Up-regulated proteins				
1a	Disulfide bond	21	3.3E − 8	VASN, LGALS3, BST1, PSAP, FAM3C, GALNT5, PRDX4, ITGB5, MXRA8, MMP14, PRKG1, MMP2, APLP2, OR1M1, LAMP1, CD59, TGFBI, PDGFRA, IGFBP3, FABP5, FN1
1b	Glycosylation site:N-linked (GlcNAc…)	25	5.9E − 9	STEAP3, VASN, BST1, PSAP, PODXL, GALNT5, ITGB5, MXRA8, CD63, CERCAM, MMP2, ASAH1, OR1M1, LAMP1, SERPINE2, CD59, PDGFRA, ITIH3, SCARB2, RCN3, IGFBP3, RCN1, TUBB3, FN1, SLC43A3
2	Transmembrane helix	25	0.015	STEAP3, VASN, CCPG1, PODXL, GALNT5, CCDC80, ITGB5, S100A10, SPPL2A, CLDN11, MXRA8, CD63, MMP14, APLP2, FTH1, ASAH1, OR1M1, SPAG9, LAMP1, SLC17A5, HMOX1, PDGFRA, SCARB2, TMEM119, SLC43A3
3	Cell junction	11	0.0012	SH3PXD2B, LPXN, SLC17A5, ANK2, SVIL, MYO1E, MAP1B, DSP, CLDN11, ADA, KCTD12
4	GO:0001525~angiogenesis	6	0.010	HMOX1, TGFBI, PLCD1, MMP14, MMP2, FN1
5	Intermediate filament	3	0.0281	DES, SYNC, VIM
6	Lysosome	8	0.0024	LAMTOR5, LAMP1, SLC17A5, PSAP, SPPL2A, SCARB2, CD63, ASAH1
7	Cell adhesion	7	0.0099	LPXN, PODXL, TGFBI, ITGB5, CERCAM, ADA, FN1
8	Extracellular matrix	4	0.072	TGFBI, CCDC80, MMP2, FN1
B. Down-regulated proteins				
1	Ribosomal protein	6	0.015	RPL35A, RPL18A, RPL22, RPL34, RPL37A, RPS23
2	Immunoglobulin domain	3	0.045	L1CAM, NEXN, MYLK
3	Fibronectin, type III/cell projection	3	0.013	L1CAM, MYLK, EPHA2
4	Antiviral defense	4	0.0045	IFIT3, IFIT2, IFIT1, GBP1
5	LIM domain	3	0.048	PDLIM5, FBLIM1, CSRP2

immediate cell counting. Cell viability calculated according to:

$$\text{Viability} = (Ct - Cnv)/Ct$$

For measurements of reduced glutathione levels (GSH), approximately 2×10^5 cells were used, and VitaBright-43 (VB-43) was used at a final concentration of 13.7 μg/mL to evaluate levels of reduced GSH [11]. The analysis was performed with excitation at 361 nm and emission at 431 nm. Cells incubated with 0.5 mmol/L Buthionine sulphoximine (BSO), an inhibitor of the gamma-glutamylcysteine synthetase, were used to determine the minimum levels of GSH for gating purposes. For cell proliferation measurements, fibroblasts from three healthy controls and three ETHE1-deficient patients were seeded at the same density and counted at 24, 36, 48 and 72 h. Cells were harvested and then diluted in PBS. The cell counting was performed on a NC-3000 image cytometer (Chemometec, Denmark), using DAPI (25 μg/ml) staining, according to the manufacturer's instructions. For cell cycle analysis, cells were grown to 70–80% confluence in DMEM with 10% FBS. 5×10^5 cells were seeded in DMEM with 0.5% fetal bovine serum (FBS) for synchronization over 48 h. The cells were then washed twice with PBS and transferred back to DMEM with 10% FBS for 24 h followed by harvesting and fixation in ethanol 70% for 18 h at −20 °C. Cell cycle progression was measured by fluorescence staining of DNA content with 1 μg/mL DAPI, 0.1% Triton X-100 in PBS. After staining, the DNA content was analyzed by the NC-3000 image cytometer and the relative percentages of cells in the G0/G1, S, and G2/M stages were determined according to manufacturer's instructions.

2.10. Mitochondrial bioenergetics measurements

Mitochondrial bioenergetics of cultured fibroblasts was measured on a Seahorse XF^e96 extracellular flux analyzer and the XF Cell Mito Stress test kit (Seahorse Bioscience, USA) as described before [16]. Briefly, 15,000 fibroblasts were seeded to each well and incubated overnight at 37 °C in a humidified atmosphere of 5% CO_2. One hour prior to the assay, culture medium was changed to unbuffered DMEM (Seahorse Bioscience) supplemented with 2 mM glutamine (Sigma Aldrich, USA), 10 mM sodium pyruvate (Gibco, USA) and 10 mM glucose (Sigma Aldrich) and the culture plate was incubated in a non-CO_2 incubator at 37 °C. Oligomycin, FCCP, and a mixture of rotenone/antimycin A were injected in a sequential manner to each well to measure mitochondrial respiration. Oxygen consumption rate (OCR) and Extracellular acidification rate (ECAR) were normalized to total protein amount measured by Bradford Protein assay (Bio-Rad).

3. Results and discussion

3.1. Phenotypic characterization of EE cells

ETHE1 deficiency causes a severe metabolic disorder affecting multiple organs, and we therefore initially measured cell viability and mitochondrial membrane potential of the cultivated EE cells using image cytometry. There was no significant difference in the percentage of viable cells between EE cells and healthy controls, with > 90% viability in both (data not shown). Neither was there any significant change in mitochondrial membrane potential (Fig. 1a).

3.2. Redox status and glutathione level

The cellular redox state was measured, since redox-related proteins such as oxidoreductases, have been described to be disrupted in ETHE1 deficient cells [6]. The fluorescent probe VitaBright-48 was applied to determine the cellular levels of the sum of free thiols of proteinic cysteines and reduced glutathione (GSH). There were no significant changes in overall thiol level (Fig. 1b). The concentration of accessible free protein-thiols in the cell can be much higher than the concentration of GSH – especially in mitochondria – and therefore it is essential to also measure GSH separately [18,19].

Glutathione (GSH) is the most abundant non-protein thiol group in mammalian cells. GSH performs many physiological functions including redox regulation and cell cycle regulation, and GSH depletion is a central signaling event, which can regulate apoptosis [20]. Cellular GSH has been specifically linked to ETHE1 and sulfide detoxification [3,21]. In a previous study we, by LC-MS/MS, measured decreased levels of both the reduced and oxidized glutathione [21]. Here, we pursue the measurements of reduced GSH by applying a GSH-specific fluorescent probe, VitaBright-43 [11]. This probe-based strategy has the advantage, over LC-MS/MS, that is measures the free, reduced GSH in living cells, and thus eliminates possible effects of the treatment of cell extracts. Fig. 1C shows that the percentage of cells with depletion of reduced GSH in EE cells is more than twofold higher than in healthy controls. This is consistent with the previous LC-MS/MS data describing that the total GSH levels, in the same patient cells, were decreased [21]. The reducing properties of sulfide can contribute to the maintained high level, with tendency to be increased, of total thiol level (Fig. 1B), whereas the specific decrease in reduced GSH level (Fig. 1C) can be an effect of glutathione's role in scavenging sulfide.

3.3. Cell growth and mitochondrial bioenergetics

Throughout the cultivation studies we noticed weaker growth for the EE cells compared with control cells, since the EE cells needed approximately three days to reach confluence compared with two days for the control cells, when seeded at same density. The increased GSH depletion and the perturbations in proteins with disulfide bonds could be central players in the observed weak growth of EE cells, since GSH can regulate, for example, cell growth and cell cycle progression [22].

3.3.1. Cell cycle

A cell cycle assay was performed to quantitate the cell distribution between the cell cycle phases: G0/G1, G2/M and S. EE and control cells exhibited very similar cell cycle distribution with 68%, 12% and 17% cells in respective phase (Fig. S1).

3.3.2. Cell growth

To further characterize cell growth we performed experiments measuring cellular duplication rate. EE cells repetitively exhibited lower cell counts than control cells, however, detailed time studies showed that mid-exponential duplication rate was in the same range as in controls, 20–27 h. See Fig. 2A for representative growth curves. Thus, neither cell cycle nor growth rate was affected. Of note, the initial cell growth was perturbed in EE cells, despite identical seeding density at time zero (Fig. 2A). After the initial 24 h the EE cells only had, on average, 55% of the cell density of the control cells ($n = 4$, $p < 0.038$) (Fig. 2B). To pinpoint this growth phenotype – impaired growth initiation – we set out to study the bioenergetics and the proteome of the EE cells.

3.3.3. Cellular bioenergetics

We performed a detailed characterization of mitochondrial bioenergetics, since mitochondria are central hubs in regulating cell activity. Seahorse metabolic analyzer was applied to measure extracellular acidification rate (ECAR) and various steps of the respiratory chain (Oxygen Consumption Rate, OCR). There was no significant change in any of the OCR parameters (Fig. S2A–C). The unaltered OCR is on one hand surprising, since ETHE1 deficiency is known to influence mitochondria, but on the other hand it is in line with the lack of OXPHOS inhibition in cultured fibroblasts [3] as well as with the unaltered mitochondrial potential measured in this study. Presence of air has been described to revert the COX-inhibition in $ETHE1^{-/-}$ tissue extracts [3], and the EE fibroblast cells were cultivated under oxidative conditions favoring relief of COX-inhibition and thus leaving OCR unaffected [3]. ECAR on the other hand was decreased by approximately

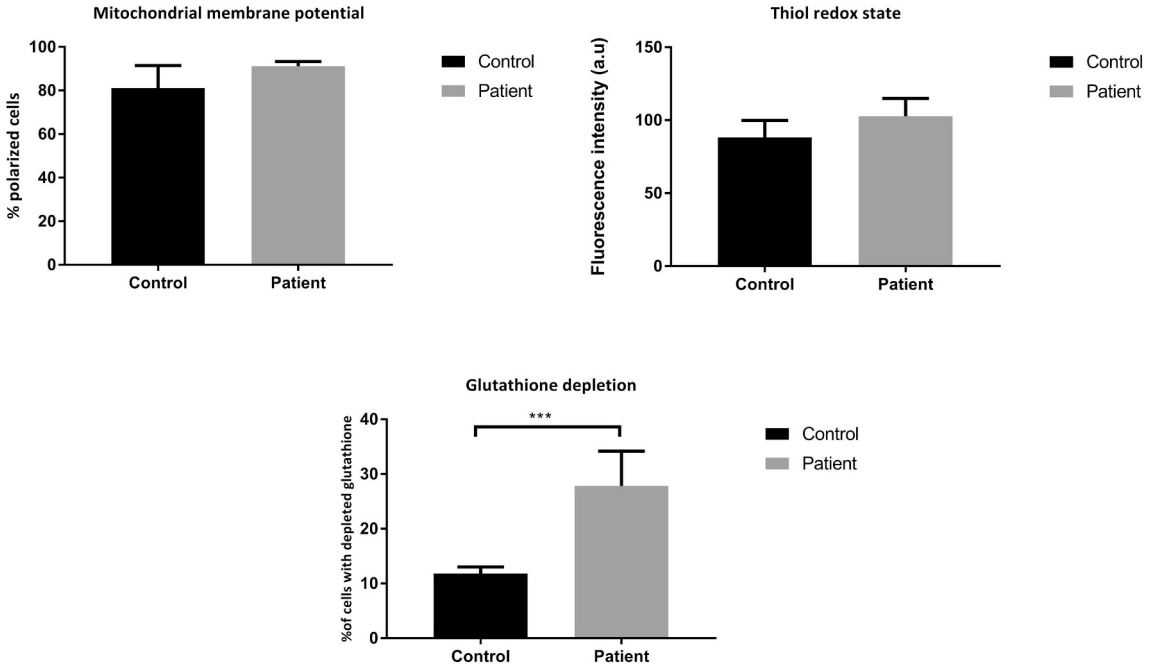

Fig. 1. Phenotypic characterization of fibroblasts derived from ETHE1-deficient patients (EE cells) and healthy controls using NC-3000 image cytometer. A) Mitochondrial membrane potential was measured after incubation with JC-1 to determine the percentage of cells with polarized mitochondria. B) Thiol redox state (TRS) was measured using VB-48. C). Glutathione status of cells. The cells were incubated with VB-43 to determine the proportion of cells with depletion of reduced glutathione. 0.5 mM of BSO (Buthionine sulphoximine), a chemical inhibitor of glutathione synthesis, was used to establish the gates that differentiate between normal levels and depleted levels. Statistical significance levels are illustrated as $p < 0.001$ ***. N = 3 error bars represent ± SEM.

30% in the ETHE1 deficient cells (Fig. S3). The extracellular acidification (measured by ECAR), mainly comes from basal glycolysis leading to lactate, especially under the applied assay conditions using glucose as substrate. ECAR measurements can be influenced by respiratory CO_2 [23], however, respiration (measured by OCR) was unaltered in the EE cells indicating that decreased lactate from glycolysis is part of the ETHE1 phenotype. Proteomics data did not present changes in glycolytic enzymes, which indicates that ECAR is regulated at the metabolite level. Our previous metabolomics study showed that the pool of NAD^+ and NADH was decreased in the same EE cells, and this can likely influence the ECAR through the NAD-dependent dehydrogenases GAPDH and LDH, which are pivotal enzymes in the pathway of lactate formation from glycolysis [21].

3.4. Proteome alterations

Large-scale proteomics analyses were performed to elucidate the changes, in proteins and pathways, associated with the perturbations related to sulfide, glutathione and the growth phenotype of the ETHE1 deficient cells. Fibroblasts were cultivated in two rounds, each followed by a separate proteomics study to minimize the risk of false discoveries. In the first and second study 6589 and 6058 proteins were detected, respectively. Combining the two data sets resulted in identification of 5432 common proteins (Fig. 3A). After applying selection criteria based on protein identification score ($p < 0.001$) and more than three quantitative peptide scans per protein (see Materials and Methods) we obtained 3562 common proteins with robust quantification (Fig. 3B).

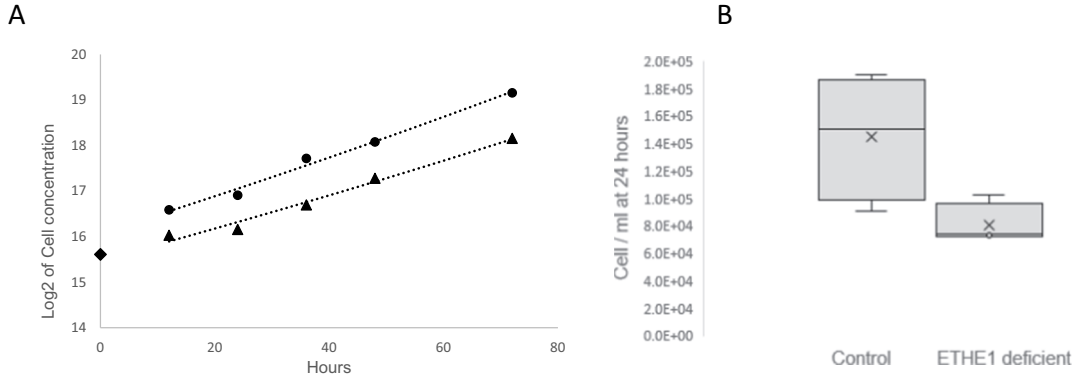

Fig. 2. Cell growth of Control vs ETHE1 deficient cells. Cell growth of Control vs ETHE1 deficient cells. A) Exponential cell growth between 12 h and 72 h for Control (circles) and ETHE1 deficient (triangles). Rhomboid indicates the initial cell concentration common for control and ETHE1 deficient cells. B) Cell concentrations reached after 24 h cultivation, when seeded at same concentrations, from four separate cultivations with one of the three control and EE cells in duplicate. One of the EE duplicates had passage number < 16, whereas all other cell cultures had < 13. Cross indicates average and whiskers indicate lowest and highest measurement. The average of the EE cells was 55% of the average of the control cells (n = 4, p = 0.038).

The quantitative data were checked for normality and found to be normally distributed (Fig. S4). The quantitative data of the 3562 proteins from the two independent studies were found to be positively correlated with a Pearson correlation coefficient above 0.74 (Fig. S5). To investigate the relationships of the proteomics patterns of the different individuals included in the two experiments we performed hierarchical cluster analysis. Cluster analysis revealed clear separation between healthy controls and patient cells in both studies (Fig. 3C and D).

To be considered as significantly differentially regulated the proteins should pass both student's *t*-test and fold change criterion. The volcano plots (Fig. 4) depict all quantitated proteins and the criteria are shown as stippled lines. 136 proteins passed the statistical criteria in both studies, 46 were down-regulated and 90 were up-regulated (Supplementary Table S2).

3.4.1. Pathway analysis of differentially regulated proteins

DAVID was applied for functional annotation clustering of the 136 significant proteins, using the 3562 common proteins as background. The most enriched functional annotations are shown in Table 1, with 8 clusters of the up-regulated proteins and 5 with the down-regulated proteins (see Supplementary Tables S3 and S4 for complete cluster data output of up- and down-regulated proteins, respectively). ETHE1 is a mitochondrial protein, however, the mitochondrial proteome was surprisingly underrepresented among the regulated pathways. In the following sections we will discuss two types of results: first, groups of proteins with functional overrepresentation, and second, single or smaller groups of proteins with pronounced fold change (FC) with putative, direct functional links to the molecular pathophysiology of ETHE1 deficiency.

3.4.2. Disulfide bonds, ER and protein glycosylation

The top two clusters from DAVID functional annotation analysis consist of up-regulated proteins with Disulfide protein bond and Glycosylation site:N-linked glycoproteins (cluster 1.A and 1.B in Table 1). The proteins of these clusters have a high degree of overlap and Supplementary Table S5 summarizes the characteristics of the 32 proteins of these clusters with regard to glycosylation and disulfide bonds. Proteins destined for secretion and cell surface exposure rely on folding via disulfide bonds and the posttranslational modification (PTM) glycosylation [24,25]. Generation of disulfide bonds is one of the major PTMs in the endoplasmic reticulum (ER) tightly connected to redox state of ER. This thiol-disulfide oxidation is catalyzed by protein disulfide isomerases (PDIs) within the ER. Two PDIs were up-regulated in our current study, PDIA5 ($p < 0.03$ and FC > 1.28 in both studies) and P4HB, also referred to as PDIA1 ($p < 0.02$ and FC > 1.25 in both studies) (Fig. 5A). Peroxiredoxin 4 (PRDX4), which also participates in hydrogen peroxide-dependent disulfide bond formation in ER was also up-regulated [26]. PRDX4 can oxidize thiol groups of PDI by using hydrogen peroxide, facilitating disulfide bonds in proteins. To validate the up-regulation of these ER redox regulators we performed western blot analyses of P4HB/PDIA1 and PRDX4, and found both to be increased in line with the proteomics data; P4HB/PDIA1 with a FC of 1.26 ($p < 0.01$) and PRDX4 with a FC of 2.2 ($p < 0.002$) (Fig. 6A, and Fig. S6A–B). Furthermore, the ER is a major dynamic Ca^{2+} repository in eukaryotic cells, and two Ca^{2+} binding proteins localized to ER, reticulocalbin 1 (RCN1) and reticulocalbin 3 (RCN3), were up-regulated (Fig. 5A).

Based on the presence of several regulated ER proteins we investigated the level of the ER chaperone BiP (HSPA5, or GRP78), which is known to be up-regulated by the ER unfolded protein response (UPR) [27]. It was not found to be regulated in our proteomics data sets (FCs of 1.07 and 1.05, with p-values above 0.2) (Supplementary Table S1). Furthermore, western blot analysis of a new set of cell samples even showed a tendency of down-regulation of BiP (HSPA5) in the EE cells (FC = 0.5, p = 0.08 and FC = 0.77, p = 0.5), all in all indicating that classical UPR is not triggered in the EE cells (Fig. 6B, and Fig. S6E–F).

Glycosylation, either as O- and N-glycosylation, are common PTMs in the ER, improving folding and facilitating secretion [28]. Cell-cell interaction is a complex process, which needs dynamic membrane environment, often regulated by glycosylation. Several proteins functioning in glycan biosynthesis and glycosaminoglycan biosynthesis were up-regulated in the ETHE1-deficient patients, namely 1, 4-alpha-glucan-branching enzyme (GBE1), Glucosamine 6-phosphate *N*-acetyltransferase (GNPNAT1), UDP-glucose6-phosphate-dehydrogenase (UGDH), Galectin-3 (LGALS3), and Polypeptide *N*-acetylgalactosaminyltransferase 5 (GALNT5) (Fig. 5B). The *N*-acetylgalactosaminyl transferase generates branched N-glycans with

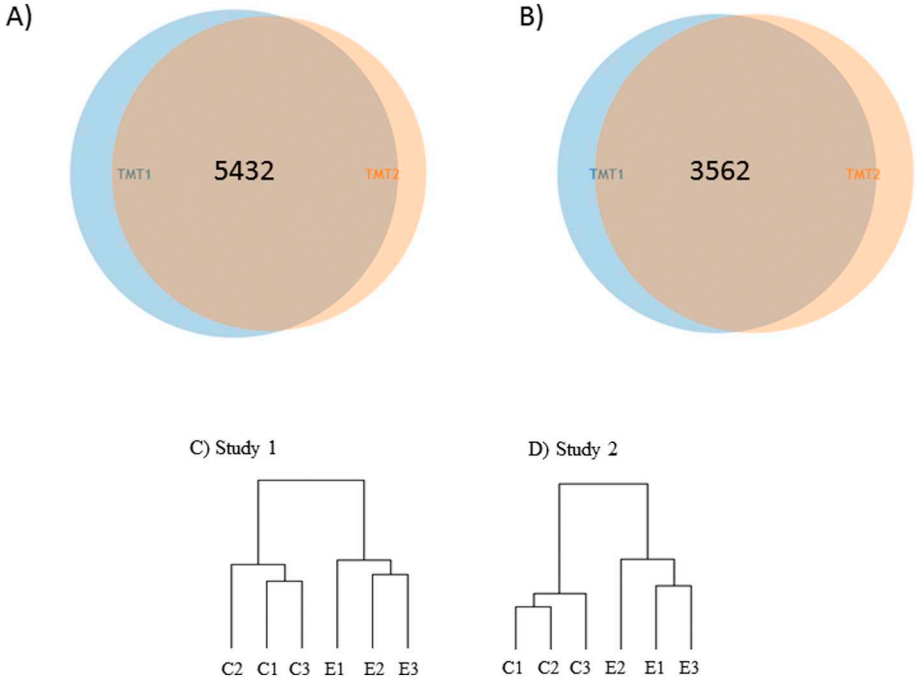

Fig. 3. Venn diagram of quantified proteins. A) > 6000 proteins were detected in both replicates of which 5432 were present in both data sets. B) 3562 common quantified proteins in the two studies with identification score ≥ 30, unique peptide scans ≥ 3. C) Hierarchical cluster analysis based on logarithmic values of 3562 common proteins was performed for TMT1 and D) for TMT2. The length of the branches and order of the individuals indicate correlation degree.

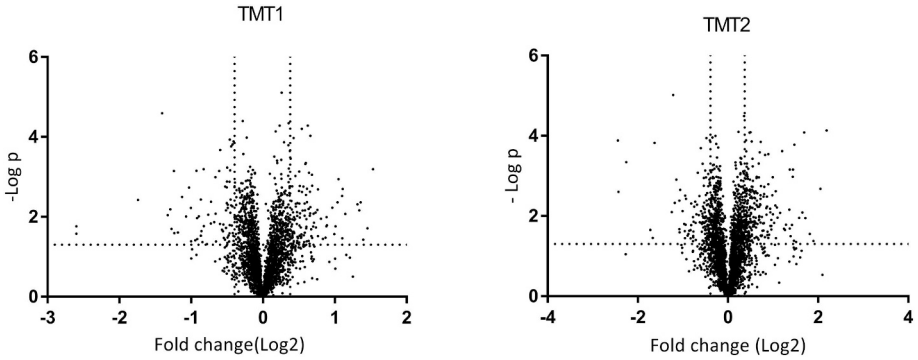

Fig. 4. Volcano plots of quantitative proteomics data from the two TMT studies.

affinities for galectins especially galectin-3 [24,29]. These branched structures are highly associated with various biological functions such as cell adhesion and migration [30–32]. Simultaneous up-regulation of galectin- 3 and fibronectin (FN1) and Integrin beta-5 (ITGB5) may imply the role of glycosylation in cell migration and fibronectin remodeling in the EE cells. Furthermore, Caveolin-1 (p value < 0.05, and the FC > 1.25) can bind to Galectin-3 and thus promoting focal adhesion, cell migration and integrin promotion [33].

Cell-cell adhesion is central for the growth of the adherent fibroblasts. The observed protein alterations related to disulfide bonds and protein glycosylation were measured in attached and actively growing fibroblasts at around 80% confluency, and phenotypic effects of these protein alterations would presumably be much stronger when present during growth initiation. The EE cells had a growth phenotype during initiation of growth (Fig. 2), and future studies are needed to clarify the specific impact of this group of proteins on growth initiation.

3.4.3. Ribosome biogenesis deregulation

Ribosomal functions are at the core of the translation machinery, and hence any change in the ribosomal proteins can affect the proliferation capacity of the cells [34]. Intriguingly, the top cluster of down-regulated proteins consist of six ribosomal proteins, including: 60S ribosomal protein L37a (RPL37A), 60S ribosomal protein L35a (RPL35A), 60S ribosomal protein L18a (RPL18A), 40S ribosomal protein S23 (RPS23), 60S ribosomal protein L34 (RPL34), and 60S ribosomal protein L22 (RPL22) (Table 1b, Fig. 5C). Supporting the observed down-regulation of ribosomal proteins, we have, in a separate metabolomics study of the same patient cells, found depleted level of the amino acids: tyrosine, methionine, tryptophan, glutamic acid, and phenylalanine [21]. We here also observed moderate down-regulation of a translational regulator Eukaryotic Initiation Factor 2 (EIF2A) with FC 0.86 and 0.78 in TMT1 and TMT2, respectively, and both p-values < 0.006 (Fig. 5D) [35]. A protein of the nutrient sensing mechanistic target of rapamycin complex 1 (mTOR1) pathway, Ragulator complex protein LAMTOR5, was found up-regulated (Fig. 5D). mTORC1 signaling is known to be activated by insulin and other growth factors [36], and Insulin-like growth factor-binding protein 3(IGFBP3) was also up-regulated. These together with slight up-regulation of LAMTOR1 and LAMTOR2 (Fig. 5D) may point to a cell compensatory mechanism to activate regulatory pathways such as mTORC1 in response to aberrant cell growth and protein synthesis [37].

mTOR is also controlled by the Ras superfamily of small GTPases [36,38]. Five members of this superfamily were up-regulated in patient cells including: Ras-associated and pleckstrin homology domains-containing protein 1(RAPH1), Ras-related protein Rab-9A (RAB9A), Ras-related protein Rab-23 (RAB23), Ras-related protein Ral-A (RALA), and Ras-related protein Rab-31 (RAB31) (Fig. 5D). These up-regulation patterns in Ras family members could be part of cellular response to regulate mTORC1 in ETHE1-deficient cells, and is consistent with previous studies clarifying Ras family functions [37,39].

3.4.4. LIM domain regulatory proteins

Three down-regulated proteins formed the LIM domain cluster, namely Cysteine and glycine-rich protein 2 (CSRP2), PDZ and LIM domain protein 5 (PDLIM5), as well as Filamin-binding LIM protein 1(FBLIM1) (Table 1 and Fig. 5E). PDZ and PDLIM5, also known as enigma homolog 1 (ENH1) [40], are involved in protein-binding interface with diverse partners including cytoskeletal components, cytoplasmic signaling proteins and transcriptional factors, indicating importance of the protein in cellular maintenance [41]. Elevated level of PDZ-LIM proteins affects cytoskeleton organization and organ development [42]. Cysteine and glycine-rich protein 2 (CSRP2) plays important roles in tissue-specific cell growth and development [43]. In line with decreased CSRP2 level is the observed up-regulation of the platelet-derived growth factor receptor alpha (PDGFRA) (Fig. 5E), which is known to suppress CSRP2 [44]. Filamin-binding LIM protein 1(FBLIM1) also known as migfilin, is responsible for cell-cell junction through actin cytoskeleton organization. FBLIM1 enables physical connections and transduces signals between extracellular and intracellular compartments, playing pivotal role in cell adhesion, shape of modulation, motility, and transcriptional regulation [45,46]. The downregulation of FBLIM1 (Fig. 5E) indicates a corrupted cell adhesion and cytoskeleton, causing deregulation of cell shape, cell motility and differentiation [45,47].

3.4.5. Single proteins with influential functions

3.4.5.1. S100 proteins, annexin A2 and AHNAK2. Among S100 family members, we detected S100A6 (also known as calcyclin) and S100A10 up-regulated in patient cells (Fig. 5F).The S100 protein family participates in a multitude of biological processes such as proliferation, migration, and cell survival by Ca^{2+} regulation [48]. S100A6 deficiency inhibits fibroblast proliferation [49] and on the other hand, S100A6 overexpression contributes to cell proliferation [50]. A S100A6 up-regulation in patient cells could be a part of cellular compensatory mechanisms to modulate cell proliferation and cell growth. Moreover, S100A10 provides a platform for membrane repair through a multiprotein complex, consisting of annexin A2 and enlarge some protein AHNAK2 [51], and these two were also up-regulated in the EE cells (Fig. 5F).

3.4.5.2. Heme oxygenase 1. Heme oxygenase 1 (HO-1) was significantly up-regulated in our study. HO-1 is a redox regulated and cytoprotective protein that catalyzes the degradation of heme to biliverdin, iron, and carbon monoxide (CO). In spite of heme's crucial functions such as oxygen transport and storage, electron transport and energy production, excess free heme is highly toxic due to its ability of causing oxidative stress, lipid peroxidation and membrane injury. Therefore, HO-1 is an important enzyme for regulating the level of the double-faced heme. ER stress induces HO-1 [52], and its product CO can in turn inhibit the sulfide synthesizing enzyme Cystathionine β-synthase (CBS) of the transsulfuration pathway [10]. Although we have

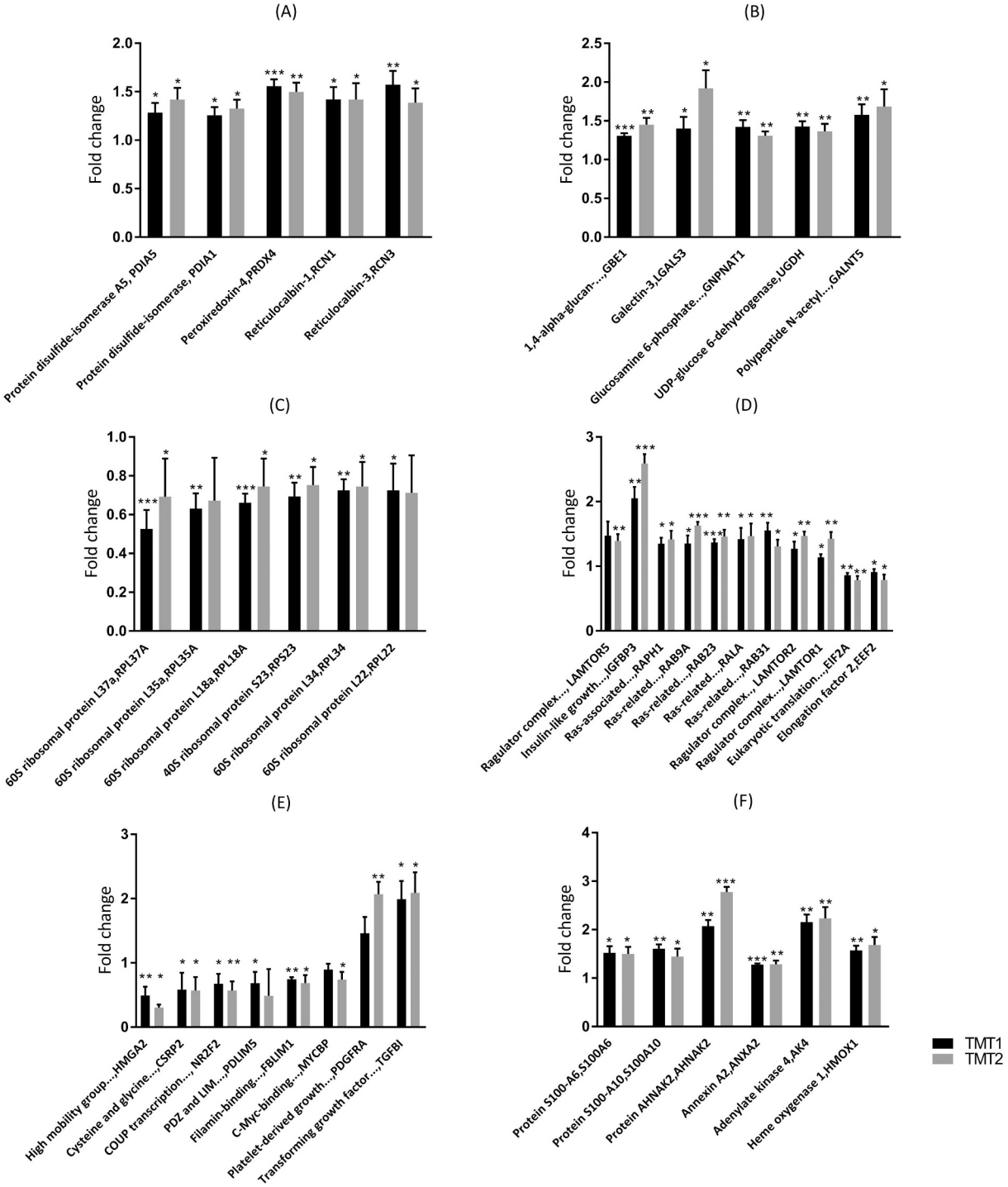

Fig. 5. Quantitative protein data of selected proteins/pathways. A) ER proteins, B) regulation of protein glycosylation, C) Ribosomal proteins, D) Translational regulation and mTOR, E) LIM domain regulatory proteins, F) S100 proteins, adenylate kinase and others.

established the links between sulfide, ER proteins and HO-1, further studies are needed to describe their dynamical interplay. Furthermore, there is a link between up-regulated HO-1 and glutathione depletion in a variety of cells, including rat brain, human fibroblasts, endothelial cells, and rat cardiomyocytes [53].

3.4.5.3. Adenylate kinase 4

Adenylate kinase 4 (AK4) was significantly up-regulated (FC > 2) in EE cells (Fig. 5F). Western blot data on AK4 support the proteomics data by exhibiting increased levels in EE cells with FC = 2.71 ($p = 0.05$) and FC = 1.71 ($p = 0.24$) in two replicate experiments (Fig. 6B and Fig. S6C–D). AK4 is a member of adenylate kinase family, located in the mitochondrial matrix, involved in energy metabolism and maintaining homeostasis of nucleotide pools via phosphorylation of AMP using either ATP or GTP as phosphate donors [54]. Recent large-scale genomic and proteomic studies have reported elevated level of AK4 under various stress conditions such as hypoxia and hydrogen peroxide induced stress [55]. Interestingly AK4 was also up-regulated in fibroblasts of short-chain acyl-CoA dehydrogenase (SCAD) deficient patients [56], revealing a new trait common for SCAD deficiency and

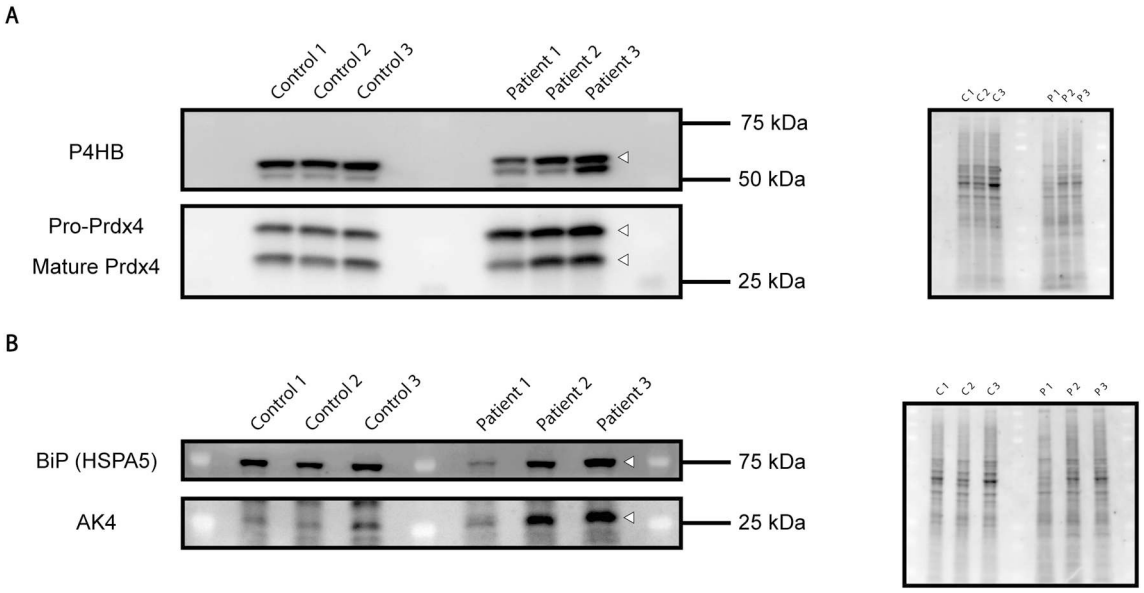

Fig. 6. Western blot analyses. The specific protein levels were quantified (left) and normalized to total protein levels (right). Fig. A) protein disulfide-isomerase (PDIA1, P4HB) and below is peroxiredoxin 4 (PRDX4), B) endoplasmic reticulum chaperone BiP (HSPA5, GRP78) and below is adenylate Kinase 4 (AK4). See Fig. S6 for additional blots and details.

ETHE1 deficiency, in addition to the SCAD dysfunction present in both conditions.

4. Conclusions

In conclusion, the study shows lower level of the redox regulator GSH in fibroblasts from ETHE1-deficient patients, which most likely is a key factor for the dysregulated cell growth. In addition, the discovery proteomics showed pronounced alterations of ribosomal proteins and proteins with disulfide bonds and glycosylation –pointing to ER redox stress with influence on protein export. The perturbation of glycosylated proteins pinpoints a possible novel link between ETHE1 deficiency and cell surface functions, such as cell adhesion, with putative effects on cell growth and tissue integrity.

Our model of cultivated patient fibroblasts, represent a milder phenotype than seen in mouse tissue studies [3,9]. Despite this, we pinpoint multiple pathways, with high importance for central cellular functions. We propose the following mechanistic model: with sufficient oxygen the sulfide level can be decreased through oxidation avoiding inhibition of OXPHOS. Reduced glutathione will be partially depleted influencing redox proteins [6]. The perturbation in sulfide and reduced glutathione levels, caused by the ETHE1 deficiency, have effects on the translational machinery, ER functions and protein glycosylation state, as well as the compendium of protein functions described in the present work.

Moreover, during the last few years there have been efforts in utilizing sulfide-releasing drugs as a potential treatment for certain medical conditions; including organ ischemia/reperfusion injury, vasodilation and atherosclerosis [57]. The output of the present study can cast light on possible cellular and biochemical side effects of such pharmacological sulfide donors.

With regard to treatment of the rare EE disorder are the pervasive effects of ETHE1 deficiency posing challenge for the design of effective treatments. Previously, partial alleviation of patient symptoms was shown by co-administration of the glutathione precursor *N*-acetylcysteine and the antibiotic metronidazole to decrease the load of sulfide-producing intestinal bacteria [3]. The recent, more advanced approach of liver transplantation has more lasting and positive effects [4], although it is likely to need support by adjuvant therapy to avoid early (pre-transplantation) neurological symptoms. The present work describes molecular effects caused by the deficiency of the persulfide dioxygenase ETHE1, and the data could be used to guide adjuvant pharmacological treatment of EE patients.

Supplementary data to this article can be found online at https://doi.org/10.1016/j.bbadis.2018.10.035.

Transparency document

The Transparency document associated with this article can be found, in online version.

Acknowledgements

We acknowledge Rasha A. Al-Saaidi for help with Seahorse metabolic analyses, and thank John and Birthe Meyer Foundation, and Department of Clinical Medicine, Aarhus University, Denmark for financial support.

References

[1] J. Palmfeldt, et al., Mitochondrial proteomics on human fibroblasts for identification of metabolic imbalance and cellular stress, Proteome Sci. 7 (2009) 20.
[2] J. Palmfeldt, P. Bross, Proteomics of human mitochondria, Mitochondrion 33 (2017) 2–14.
[3] V. Tiranti, et al., Loss of ETHE1, a mitochondrial dioxygenase, causes fatal sulfide toxicity in ethylmalonic encephalopathy, Nat. Med. 15 (2) (2009) 200–205.
[4] V. Tiranti, et al., Ethylmalonic encephalopathy is caused by mutations in ETHE1, a gene encoding a mitochondrial matrix protein, Am. J. Hum. Genet. 74 (2) (2004) 239–252.
[5] A. Drousiotou, et al., Ethylmalonic encephalopathy: application of improved biochemical and molecular diagnostic approaches, Clin. Genet. 79 (4) (2011) 385–390.
[6] J. Palmfeldt, et al., Proteomics reveals that redox regulation is disrupted in patients with ethylmalonic encephalopathy, J. Proteome Res. 10 (5) (2011) 2389–2396.
[7] N. Gregersen, J. Hansen, J. Palmfeldt, Mitochondrial proteomics-a tool for the study of metabolic disorders, J. Inherit. Metab. Dis. 35 (4) (2012) 715–726.
[8] T.M. Hildebrandt, et al., Proteome adaptations in Ethe1-deficient mice indicate a role in lipid catabolism and cytoskeleton organization via post-translational protein modifications, Biosci. Rep. 33 (2013) 575–584.
[9] N. Sahebekhtiari, et al., Quantitative proteomics suggests metabolic reprogramming during ETHE1 deficiency, Proteomics 16 (7) (2016) 1166–1176.
[10] O. Kabil, N. Motl, R. Banerjee, H2S and its role in redox signaling, Biochim. Biophys. Acta Protein Proteomics 1844 (8) (2014) 1355–1366.
[11] M.E. Skindersoe, S. Kjaerulff, Comparison of three thiol probes for determination of apoptosis-related changes in cellular redox status, Cytometry A 85 (2) (2014) 179–187.

[12] M.J. de Hoon, et al., Open source clustering software, Bioinformatics 20 (9) (2004) 1453–1454.
[13] A.J. Saldanha, Java Treeview—extensible visualization of microarray data, Bioinformatics 20 (17) (2004) 3246–3248.
[14] D.W. Huang, B.T. Sherman, R.A. Lempicki, Systematic and integrative analysis of large gene lists using DAVID bioinformatics resources, Nat. Protoc. 4 (1) (2009) 44–57.
[15] J.A. Vizcaino, et al., 2016 update of the PRIDE database and its related tools, Nucleic Acids Res. 44 (22) (2016) 11033.
[16] A.S. Bie, et al., Effects of a mutation in the HSPE1 gene encoding the mitochondrial co-chaperonin HSP10 and its potential association with a neurological and developmental disorder, Front. Mol. Biosci. 3 (2016) 65.
[17] M.E. Skindersoe, M. Rohde, S. Kjaerulff, A novel and rapid apoptosis assay based on thiol redox status, Cytometry A 81A (5) (2012) 430–436.
[18] R. Requejo, et al., Cysteine residues exposed on protein surfaces are the dominant intramitochondrial thiol and may protect against oxidative damage, FEBS J. 277 (6) (2010) 1465–1480.
[19] M.P. Murphy, Mitochondrial thiols in antioxidant protection and redox signaling: distinct roles for glutathionylation and other thiol modifications, Antioxid. Redox Signal. 16 (6) (2012) 476–495.
[20] R. Franco, J.A. Cidlowski, Glutathione efflux and cell death, Antioxid. Redox Signal. 17 (12) (2012) 1694–1713.
[21] N. Sahebekhtiari, et al., Untargeted metabolomics analysis reveals a link between ETHE1-mediated disruptive redox state and altered metabolic regulation, J. Proteome Res. 15 (5) (2016) 1630–1638.
[22] J.L. Garcia-Gimenez, et al., Nuclear glutathione, Biochim. Biophys. Acta Gen. Subj. 1830 (5) (2013) 3304–3316.
[23] S.A. Mookerjee, et al., The contributions of respiration and glycolysis to extracellular acid production, Biochim. Biophys. Acta 1847 (2) (2015) 171–181.
[24] C. Boscher, J.W. Dennis, I.R. Nabi, Glycosylation, galectins and cellular signaling, Curr. Opin. Cell Biol. 23 (4) (2011) 383–392.
[25] M. Hagiwara, K. Nagata, Redox-dependent protein quality control in the endoplasmic reticulum: folding to degradation, Antioxid. Redox Signal. 16 (10) (2012) 1119–1128.
[26] T.J. Tavender, J.J. Springate, N.J. Bulleid, Recycling of peroxiredoxin IV provides a novel pathway for disulphide formation in the endoplasmic reticulum, EMBO J. 29 (24) (2010) 4185–4197.
[27] K. Yamamoto, et al., Transcriptional induction of mammalian ER quality control proteins is mediated by single or combined action of ATF6alpha and XBP1, Dev. Cell 13 (3) (2007) 365–376.
[28] A. Varki, J.D. Esko, K.J. Colley, Cellular organization of glycosylation, in: A. Varki, et al. (Eds.), Essentials of Glycobiology, Cold Spring Harbor, NY, 2009.
[29] S.K. Patnaik, et al., Complex N-glycans are the major ligands for galectin-1, -3, and -8 on Chinese hamster ovary cells, Glycobiology 16 (4) (2006) 305–317.
[30] D. Bironaite, et al., N-glycans influence the in vitro adhesive and invasive behaviour of three metastatic cell lines, Tumor Biol. 21 (3) (2000) 165–175.
[31] Y.Y. Zhao, et al., Branched N-glycans regulate the biological functions of integrins and cadherins, FEBS J. 275 (9) (2008) 1939–1948.
[32] Y.Y. Zhao, et al., Functional roles of N-glycans in cell signaling and cell adhesion in cancer, Cancer Sci. 99 (7) (2008) 1304–1310.
[33] J.G. Goetz, et al., Concerted regulation of focal adhesion dynamics by galectin-3 and tyrosine-phosphorylated caveolin-1, J. Cell Biol. 180 (6) (2008) 1261–1275.
[34] D. Ruggero, P.P. Pandolfi, Does the ribosome translate cancer? Nat. Rev. Cancer 3 (3) (2003) 179–192.
[35] E. Kim, et al., eIF2A, an initiator tRNA carrier refractory to eIF2alpha kinases, functions synergistically with eIF5B, Cell. Mol. Life Sci. 75 (23) (2018) 4287–4300.
[36] C.G. Proud, Control of the translational machinery by amino acids, Am. J. Clin. Nutr. 99 (1) (2014) 231s–236s.
[37] L. Li, et al., Regulation of mTORC1 by the Rab and Arf GTPases, J. Biol. Chem. 285 (26) (2010) 19705–19709.
[38] J.L. Jewell, K.L. Guan, Nutrient signaling to mTOR and cell growth, Trends Biochem. Sci. 38 (5) (2013) 233–242.
[39] T. Maehama, et al., RalA functions as an indispensable signal mediator for the nutrient-sensing system, J. Biol. Chem. 283 (50) (2008) 35053–35059.
[40] J.L. Kadrmas, M.C. Beckerle, The LIM domain: from the cytoskeleton to the nucleus, Nat. Rev. Mol. Cell Biol. 5 (11) (2004) 920–931.
[41] N. Nakagawa, et al., ENH, containing PDZ and LIM domains, heart/skeletal muscle-specific protein, associates with cytoskeletal proteins through the PDZ domain, Biochem. Biophys. Res. Commun. 272 (2) (2000) 505–512.
[42] I. Bach, The LIM domain: regulation by association, Mech. Dev. 91 (1–2) (2000) 5–17.
[43] R. Weiskirchen, et al., LIM-domain protein cysteine- and glycine-rich protein 2 (CRP2) is a novel marker of hepatic stellate cells and binding partner of the protein inhibitor of activated STAT1, Biochem. J. 359 (2001) 485–496.
[44] M.K. Jain, et al., Molecular cloning and characterization of SmLIM, a developmentally regulated LIM protein preferentially expressed in aortic smooth muscle cells, J. Biol. Chem. 271 (17) (1996) 10194–10199.
[45] Y.Z. Tu, et al., Migfilin and Mig-2 link focal adhesions to filamin and the actin cytoskeleton and function in cell shape modulation, Cell 113 (1) (2003) 37–47.
[46] H. Akazawa, et al., A novel LIM protein Cal promotes cardiac differentiation by association with CSX/NKX2-5, J. Cell Biol. 164 (3) (2004) 395–405.
[47] J.P. Zhao, et al., Migfilin interacts with Src and contributes to cell-matrix adhesion-mediated survival signaling, J. Biol. Chem. 284 (49) (2009) 34308–34320.
[48] A.R. Bresnick, D.J. Weber, D.B. Zimmer, S100 proteins in cancer, Nat. Rev. Cancer 15 (2) (2015) 96–109.
[49] E.C. Breen, K. Tang, Calcyclin (S100A6) regulates pulmonary fibroblast proliferation, morphology, and cytoskeletal organization in vitro, J. Cell. Biochem. 88 (4) (2003) 848–854.
[50] R. Hwang, et al., Calcyclin, a Ca^{2+} ion-binding protein, contributes to the anabolic effects of simvastatin on bone, J. Biol. Chem. 279 (20) (2004) 21239–21247.
[51] A. Rezvanpour, L. Santamaria-Kisiel, G.S. Shaw, The S100A10-Annexin A2 complex provides a novel asymmetric platform for membrane repair, J. Biol. Chem. 286 (46) (2011) 40174–40183.
[52] X.M. Liu, et al., Endoplasmic reticulum stress stimulates heme oxygenase-1 gene expression in vascular smooth muscle. Role in cell survival, J. Biol. Chem. 280 (2) (2005) 872–877.
[53] R. Foresti, et al., Thiol compounds interact with nitric oxide in regulating heme oxygenase-1 induction in endothelial cells - involvement of superoxide and peroxynitrite anions, J. Biol. Chem. 272 (29) (1997) 18411–18417.
[54] C. Panayiotou, et al., Evidence of an intact N-terminal translocation sequence of human mitochondrial adenylate kinase 4, Int. J. Biochem. Cell Biol. 42 (1) (2010) 62–69.
[55] R.J. Liu, et al., Enzymatically inactive adenylate kinase 4 interacts with mitochondrial ADP/ATP translocase, Int. J. Biochem. Cell Biol. 41 (6) (2009) 1371–1380.
[56] A.V. Edhager, et al., Proteomic investigation of cultivated fibroblasts from patients with mitochondrial short-chain acyl-CoA dehydrogenase deficiency, Mol. Genet. Metab. 111 (3) (2014) 360–368.
[57] B. Olas, Gasomediators (·NO, CO, and H(2)S) and their role in hemostasis and thrombosis, Clin. Chim. Acta 445 (2015) 115–121.